DEC 15 2000

SANDIA REPORT

SAND2000-3044
Unlimited Release
Printed December 2000

Lightning Induced Arcing : An LDRD Report

Roy E. Jorgenson, Larry K. Warne, and Erich E. Kunhardt

Prepared by
Sandia National Laboratories
Albuquerque, New Mexico 87185 and Livermore, California 94550

Sandia is a multiprogram laboratory operated by Sandia Corporation, a Lockheed Martin Company, for the United States Department of Energy under Contract DE-AC04-94AL85000.

Approved for public release; further dissemination unlimited.

Sandia National Laboratories

Issued by Sandia National Laboratories, operated for the United States Department of Energy by Sandia Corporation.

NOTICE: This report was prepared as an account of work sponsored by an agency of the United States Government. Neither the United States Government, nor any agency thereof, nor any of their employees, nor any of their contractors, subcontractors, or their employees, make any warranty, express or implied, or assume any legal liability or responsibility for the accuracy, completeness, or usefulness of any information, apparatus, product, or process disclosed, or represent that its use would not infringe privately owned rights. Reference herein to any specific commercial product, process, or service by trade name, trademark, manufacturer, or otherwise, does not necessarily constitute or imply its endorsement, recommendation, or favoring by the United States Government, any agency thereof, or any of their contractors or subcontractors. The views and opinions expressed herein do not necessarily state or reflect those of the United States Government, any agency thereof, or any of their contractors.

Printed in the United States of America. This report has been reproduced directly from the best available copy.

Available to DOE and DOE contractors from
U.S. Department of Energy
Office of Scientific and Technical Information
P.O. Box 62
Oak Ridge, TN 37831

Telephone: (865)576-8401
Facsimile: (865)576-5728
E-Mail: reports@adonis.osti.gov
Online ordering: http://www.doe.gov/bridge

Available to the public from
U.S. Department of Commerce
National Technical Information Service
5285 Port Royal Rd
Springfield, VA 22161

Telephone: (800)553-6847
Facsimile: (703)605-6900
E-Mail: orders@ntis.fedworld.gov
Online order: http://www.ntis.gov/ordering.htm

DISCLAIMER

Portions of this document may be illegible in electronic image products. Images are produced from the best available original document.

RECEIVED
DEC 22 2000
OSTI

SAND2000-3044
Unlimited Release
Printed December 2000

Lightning Induced Arcing: An LDRD Report

Roy E. Jorgenson and Larry K. Warne
Electromagnetics and Plasma Physics Analysis Dept.
Sandia National Laboratories
P. O. Box 5800
Albuquerque, NM 87185-1152

Prof. Erich E. Kunhardt
Department of Physics
Stevens Institute of Technology
Hoboken, NJ 07030

Abstract

The purpose of this research was to develop a science-based understanding of the early-time behavior of electric surface arcing in air at atmospheric pressure. As a first step towards accomplishing this, we used a kinetic approach to model an electron swarm as it evolved in a neutral gas under the influence of an applied electric field. A computer code was written in which pseudo-particles, each representing some number of electrons, were accelerated by an electric field. The electric field due to the charged particles was calculated efficiently using a tree algorithm. Collision of the electrons with the background gas led to the creation of new particles through the processes of ionization and photoionization. These processes were accounted for using measured cross-section data and Monte Carlo methods. A dielectric half-space was modeled by imaging the charges in its surface. Secondary electron emission from the surface, resulting in surface charging, was also calculated. Simulation results show the characteristics of a streamer in three dimensions. A numerical instability was encountered before the streamer matured to form branching.

Acknowledgment

The authors would like to thank Harold P. Hjalmarson for sharing his knowledge on band gap effects and Robert A. Anderson for sharing his knowledge on secondary electron emission and measurement techniques.

Contents

1 Introduction 7

1.1 Description of the Breakdown Process 7

1.2 Past Work 8

1.3 Problem Description 9

2 Code Description 10

2.1 Picking the Time Step 10

2.2 Electric Field Update 11

2.3 Pushing the Electrons 12

2.4 Electrons Colliding with Neutrals 13

2.5 Surface Interactions 19

2.6 Particle Renormalization 20

3 Results 21

3.1 Breakdown Through a Volume, Photoionization Off 21

3.2 Breakdown Through a Volume, Photoionization On 21

4 Experiments 27

5 Problem Areas 29

6 Future Work 32

7 Conclusion 32

Figures

1 Problem Geometry 9

2 Stacked Collision Frequencies 15

3 Center of Mass and Laboratory Coordinates 16

4 Center of Mass Coordinates Viewed Along Direction of Primary Electron 17

5 Secondary Electron Emission Curve 19

6 Number of Electrons vs. Time 22

7 E_z at Each Electron vs. z 23

8 Electron Cloud as Viewed Along $\hat{x}$ 24

9 Electron Cloud as Viewed Along $\hat{y}$ 25

10 Electron Cloud as Viewed Along $\hat{z}$ 26

11 E_z at Each Electron vs. z with Photoionization On 27

12 Electron Cloud as Viewed Along $\hat{x}$ with Photoionization On 28

13 E_z at Each Electron vs. z Showing Onset of Instability 29

14 Detail of Instability Region 30

15 Source and Observation Clouds 31

Lightning Induced Arcing: An LDRD Report

1 Introduction

The goal of this project was to develop a science-based understanding of the early-time behavior of high-voltage electric breakdown that occurs in air at atmospheric pressure. In particular, we are interested in surface flashover, where breakdown occurs across a dielectric surface. Our interest in these matters stems from the fact that we are responsible for answering questions about lightning environments as they apply to weapon safety. Frequently, these questions demand an understanding of electrical arcing in order to determine if lightning will cause arcing to a benign object, such as a weapon case, or to a nuclear safety critical component. A large number of lightning-caused arcing situations related to safety involve high-voltage arcing in the presence of one or more dielectric surfaces. Some examples are: arcing through cracks in cable insulation or across the face of a connector from pin to connector body (two planar surfaces), arcing through pin holes in cable insulation (a surrounding surface), or arcing across a dielectric isolator (a single surface).

Presently, empirical data (combined with large safety margins) is used to support safety assessments, whenever possible. The use of empirical data is unsatisfactory, however, because the data usually does not exist for the particular situation that we are interested in and without an understanding of the underlying physics we cannot extrapolate the data with the confidence level needed by nuclear safety unless we resort to using gross upper bounds. It is important to develop our understanding of the arcing process because the use of gross upper bounds can lead to a situation where we are forced to require additional layers of protection, which increases the cost and complexity of an operation.

1.1 Description of the Breakdown Process

Breakdown in gas, without a surface present, is explained by one of two models. At low pressures ($pd < 200$ Torr-cm, where p is the pressure and d is the gap distance), the Townsend model is valid. At higher pressures, the Townsend model becomes invalid and we must turn to a streamer model in order to explain the results [1]. Since breakdown at atmospheric pressure (p =760 Torr) is our primary concern, and our gaps are usually on the order of one centimeter or larger, we are interested in modeling the streamer breakdown process.

In breakdown, an electron is accelerated by an electric field, collides with the background neutral gas molecules, ionizes the molecules and creates new electrons. These new electrons are then also accelerated by the electric field and further ionize gas molecules. The number of electrons (n) in the problem space grows exponentially ($n = n_0 e^{\alpha x}$), leading

to what is known as an electron avalanche. Eventually, the number of electrons and ions in the problem space become so great that their field modifies the applied electric field. At this point we say that the electron swarm has transitioned from the avalanche stage into the streamer stage. In a uniform field, and only in a uniform field, it has been found experimentally that the avalanche-to-streamer transition necessarily leads to a total breakdown of the gap [2].

The electric field ahead of the streamer is greater than the applied field, while inside the body of the streamer, the electric field is smaller than the applied field. Small changes in the electric field cause the growth rate of the electrons (α) to change by a large amount. Therefore, electrons will form in the head of the streamer faster than in the applied field alone, but will form in the body of the streamer slower than in the applied field alone. Since the majority of the electrons are in the body, the overall growth rate of the electrons will decrease when the avalanche-to-streamer transition occurs [3].

At the same time that ionizations are occurring, the gas molecules are being excited by collision and release photons of various energies. These photons travel in all directions and are absorbed at various distances from their origin. Some of the high energy photons lead to photoionization and the subsequent formation of new electrons at locations removed from the main avalanche. These electrons are the seeds of secondary avalanches and streamers. The secondary streamers coalesce, which contributes to the branched appearance of the breakdown [2]. Instabilities in the ionization front may also contribute to the appearance of branching.

1.2 Past Work

It is difficult to find consistent information on the effect of a dielectric surface on breakdown strength. Much of the information on breakdown in atmospheric air comes from the power industry and is mainly empirical in nature. One paper notes that the breakdown strength of a uniform field gap with a right cylinder dielectric spacer is roughly half the breakdown strength of the gap without the spacer for a 50 Hz voltage waveform [5]. In the literature on vacuum breakdown, which has a much better scientific basis than that of the power industry, there is general agreement that breakdown will occur preferentially across an insulator surface that bridges the gap between two electrodes. In a vacuum the breakdown process consists of three stages: (1) There is an emission of electrons from the triple junction (the junction between electrode, dielectric and vacuum) that initiates the breakdown. (2) There is a development of the discharge, which causes gas to be desorbed from the insulator's surface. (3) The breakdown occurs within the desorbed gas by either a Townsend or streamering process [6].

Since the processes in the vacuum literature were well developed, we used them as a guide to determine the processes needed in our problem. The triple point emission is thought to occur due to imperfections in the mating between the dielectric spacer and the electrode leading to high field regions that enhance the number of electrons being emitted from the electrode. The geometry of these imperfections are difficult to quantify. There

is further uncertainty as to what causes the emission from the electrode in the first place, whether it is a microscopic whisker that enhances the field at the emission site or a small speck of oxide that acts as a catalyst [7]. Because of the uncertainty concerning the triple point we decided not to model the electrodes in the problem and merely postulate the existence of an initial swarm of electrons. Not modeling the electrodes has the added benefit of simplifying the field calculations. There is much contention over what constitutes the second stage of the vacuum breakdown process, but the most accepted theory is that an electron avalanche propagates across the dielectric surface and causes gas to desorb from the surface. The avalanche is caused by secondary emission electrons being released by the impact of primary electrons on the surface [8]. We included secondary electron emission from the surface as a source of electrons and as a surface charging mechanism in our problem. We did not, however, model the desorption of gas from the surface since, unlike desorption in a vacuum, the increase in gas density over the density at atmospheric pressure is relatively low [9]. The only way that a desorbed gas could influence the breakdown process is if it were of such a species that small amounts could function as a catalyst in the background gas so that the mixture has a lower breakdown voltage.

1.3 Problem Description

The geometries that we are actually concerned with involve breakdown across complex surfaces with complex electrodes that lead to the presence of highly nonuniform fields. In order to study the fundamental physical processes, we will simplify the geometry to one of an infinite dielectric half-space with no electrodes as shown in Figure 1. A uniform electric field, $\overline{E}_{inc} = \hat{z}E_{inc}$ is applied parallel to the surface of the dielectric half-space, which fills the region $x \leq 0$. At time $t = 0$, a small number of initial electrons (~ 10), uniformly distributed in a small sphere about the origin (radius $\sim 1\mu$m), are allowed to move in the electric field. We track the progress of each individual electron using the computer code described below. We can thus observe the behavior of the electron swarm as the breakdown develops.

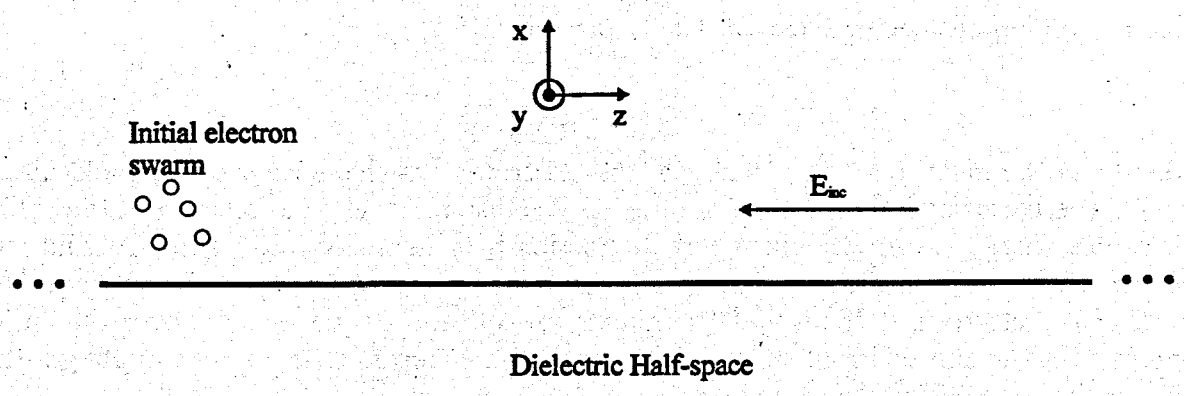

1. Problem Geometry

2 Code Description

The code that we wrote to study breakdown falls into the general category of particle codes [10][11]. We chose the particle approach because of its flexibility – as long as we account for the microscopic interactions of the particles, we can model the macroscopic behavior. We first impose a temporal grid on the time variable, discretizing it into uniform time steps Δt. Because the mass of the electron is much smaller than the mass of the ion, at early time, the ions can be approximated as standing still and we can concentrate only on movement of the electrons [4]. At each time step we first calculate the electric field that exists at each electron due to the applied field and due to the field whose sources are the other charged particles in the problem space. We then update the position and velocity of each electron by integrating its equations of motion over the time step Δt, using the force due to the electric field. Next, we use measured cross-section data and Monte Carlo methods to determine if the electron collided with a molecule of the background gas in the preceding timestep. If a collision did take place, we determine if the collision was elastic, excitational or ionizing. If the collision was ionizing, new charged particles (at least a single electron-ion pair) enter the problem space in the next time step. If a dielectric surface is present, the electron can collide with it and either attach to it or release electrons from it. With new electrons and ions having the chance to enter the problem space at each time step, the number of charged particles can become large enough to overwhelm the computer. As the number of electrons or ions exceeds a given limit, the particles are renormalized such that each particle in the problem space represents a group of actual particles. The program then proceeds to the next time step where the above sequence repeats itself. The following sections discuss each of the major steps of the code in detail.

2.1 Picking the Time Step

First we must establish the time step (Δt) for the code. The collision frequency $\nu(\epsilon)$ for an electron colliding with a background gas molecule is defined as the number of collisions an electron undergoes per unit time (usually per second) [2]

$$\nu(\epsilon) = \overline{\mathrm{v}} N \sigma(\epsilon) \tag{1}$$

where $\overline{\mathrm{v}}$ is the mean random velocity of the electron, N is the density of gas molecules and $\sigma(\epsilon)$ is the cross-section of the electron-neutral collision, which is a function of the colliding electron's energy ϵ. As we will see in the section below entitled "Electrons Colliding with Neutrals", we have measured data for $\sigma(\epsilon)$ and we know that $\overline{\mathrm{v}} = \sqrt{2\epsilon/m}$, where m is the mass of the electron. If we find the maximum collision frequency $\nu_{\max}$ over the entire energy range of the electron, then we can set the time step so that we are sampling m times the maximum collision frequency or

$$\Delta t = \frac{1}{\nu_{\max} m}$$

The value chosen for m must be much greater than one (in all of our simulations we chose

$m = 10$) so that the collision probability, discussed later in the section entitled "Electrons Colliding with Neutrals", is accurate.

2.2 Electric Field Update

As we will discover in the section below entitled "Pushing the Electrons", we can ignore the effect of the magnetic field when moving the electron and concentrate only on the electric field. The electric field that applies the accelerating force to a particular electron has two contributions

$$\overline{E} = \overline{E}_{inc} + \overline{E}_{part}$$

where $\overline{E}_{inc}$ is the applied field and $\overline{E}_{part}$ is the field due to all charged particles in the problem space other than the electron where we are observing (the electron's own field does not apply a force to it). In this code we calculate the field differently than the way traditionally used in particle-in-cell (PIC) codes [10][11], namely, where a grid is imposed on the problem space, the particles are mapped onto the grid via a charge density, the field is calculated from the charge density using Poisson's equation and the field is mapped onto the particles from the grid. Rather, we will use a hierarchical tree method as described in [12], which allows us to perform the field calculation without using a grid. Tree methods are advantageous in problems where there is no boundary and where the particle distribution is strongly nonuniform. We know that the streamer exhibits a large concentration of electrons in its head as opposed to its body. Also as branching occurs, there are large contrasts between the number of particles in the branches versus the number of particles between the branches. The tree method allows us to concentrate our computational resources in regions where particles exist and ignore regions of empty space.

The algorithm to update the electric field at an electron is divided into three parts. First, we must build the tree data structure. Second, we must calculate the charge and center of charge for each level of the tree. Finally, we must calculate the field at each electron.

In order to build the tree data structure we first find a box with dimensions large enough to enclose all the charged particles in the problem space and call it the "root". We then divide each dimension of the box in half to form eight daughter cells. For each daughter cell we determine the number of particles that are located within. If the cell is empty, it is ignored. If the cell contains one particle, it is stored as a "leaf" in the tree structure. The center of charge of the leaf is the location of the single particle and the charge of the leaf is the charge of the single particle. If there is more than one particle in the cell, it is stored as a "twig" and the twig is further subdivided into eight daughters. The process continues until each particle has been assigned to its own leaf. Since ionizing collisions can occur in the time step preceding the field update, it is possible to have three collocated particles in a cell: the original electron, and an electron-ion pair from the neutral. The algorithm needs to exit if all particles within a cell are collocated in order to avoid an infinite loop. Later, during the field update this means that we do not account for the field on a particle due to other collocated particles. This should be the case only for one time step until the collocated particles can move far enough away from each other that each particle is assigned

a separate leaf.

The charge for each twig is found by adding the charge of each of its daughters. The center of charge is computed by adding the center of charge of each daughter weighted by the number of particles the daughter contains. The calculation progresses from the leaves of the tree to the root.

When calculating the field at the ith electron we start at the tree root. For each twig j we take the ratio between the length of the twig's side S_j and the distance between the observation electron and the center of charge of the twig $|\overline{r_{ij}}|$. If the ratio is less than a user-defined criterion θ, the internal structure of the twig is ignored and the electric field at electron i due to the twig j is

$$\overline{E_j}(i) = \frac{q_j}{4\pi\varepsilon_0}\frac{\overline{r_{ij}}}{|\overline{r_{ij}}|^3} \tag{2}$$

where q_j is the charge of the twig and ε_0 is the permittivity of free space. This field is added to the cumulative total for the observation electron. If the ratio $S_j/|\overline{r_{ij}}| > \theta$, then each of the twig's daughters is checked against θ and the process continues until the criterion is fulfilled, or until we reach a leaf. More details of the tree method can be found in [12].

The electric field update is where the code spends the vast majority of run time. The field can be updated at each time step, or time steps can be skipped between field updates at the user's discretion. Within the field update, the majority of time (~95%) is spent in the subroutine that calculates the field at each particle; building the tree and calculating the charge is cheap by comparison. If there are M charged particles in the problem space, the field update is done in $\sim M \log M$ operations. If θ is allowed to approach 0, the operation count increases to $\sim M^2$ because the algorithm must traverse the tree down to the leaf level in order to satisfy θ. For all the results shown here, $\theta = 0.5$, which is conservative. We used recursion to implement all aspects of the field update.

If an infinite, half-space dielectric is present, filling the space $x < 0$, then each charged particle q located at (x, y, z) has an image particle located at $(-x, y, z)$. The image particle has a charge of

$$q' = \frac{1-\epsilon_r}{1+\epsilon_r}q$$

where ϵ_r is the relative permittivity of the dielectric.

2.3 Pushing the Electrons

The equations of motion for an electron are

$$m\frac{d\overline{v}}{dt} = \overline{F}$$

$$\frac{d\overline{x}}{dt} = \overline{v}$$

where m is the mass of the electron, $\overline{v}$ is its velocity, $\overline{x}$ is its position, $\overline{F}$ is the force on the electron, and t is time. Finite-differencing these equations allows us to update the velocity

and position using the leap-frog method:

$$\overline{v}_{new} = \overline{v}_{old} + \frac{\overline{F}_{old}}{m}\Delta t$$
$$\overline{x}_{new} = \overline{x}_{old} + \overline{v}_{new}\Delta t$$

where $\overline{v}_{new}$ is calculated at a time $\Delta t/2$ later than the known quantities $\overline{x}_{old}$ and $\overline{F}_{old}$. In order to start the entire process, we interpolate $v(0)$ back in time to $v(-\Delta t/2)$ using $F(0)$ [10].

The force on the particle is due to both electric and magnetic fields

$$\overline{F} = q\overline{E} + q(\overline{v} \times \overline{B})$$

However, the source of the magnetic field $\overline{B}$ is an electric current. At early time when the electron density is small, the electric currents are also small and the generated magnetic field can be ignored.

2.4 Electrons Colliding with Neutrals

For collisions, the code follows the method outlined in [13]. At early time, the ion and electron densities are small enough that we can ignore collisions between electrons and ions or collisions between electrons. Therefore, we only have to concern ourselves with the probability of the electrons colliding with the background gas neutrals and further with the probability of collision type: elastic, excitational, or ionizing. The probability of a collision occurring at time t is

$$P(t) = 1 - e^{-\int_0^t \nu(\epsilon)dt} \tag{3}$$

where $\nu(\epsilon)$ is the collision frequency (1). Since the electron is accelerated in the electric field, its energy continuously changes with respect time, and thus, finding $P(t)$ becomes difficult. We have to use a small enough time step that the electron has an approximately constant energy over its time step, and therefore, its collision frequency $\nu(\epsilon)$ is approximately constant. We could then perform the integral over a particular time step analytically:

$$P(\Delta t) = 1 - e^{-\nu\Delta t} \approx \nu\Delta t \qquad \text{if } \nu\Delta t \ll 1 \tag{4}$$

Equation (4) emphasizes the fact that the timestep must be small in order to make the probability of multiple collisions between time steps vanishingly small. This is accomplished by using a large value of m in choosing the time step, as discussed previously. A collision takes place if a random number, uniformly distributed on the interval [0,1] is less than $P(\Delta t)$. For each particle and at each time step, we have to make this check, which leads to a large amount of computation.

We can alleviate this amount of calculation by using the null-event method [15]. The collision frequency is composed of a sum of N sub-process collision frequencies (elastic, excitational, ionizing etc...):

$$\nu(\epsilon) = \nu_{el}(\epsilon) + \nu_{ex}(\epsilon) + \nu_{ion}(\epsilon) + ... + \nu_N(\epsilon)$$

We will add one more process to the sum, the "null-collision" process (ν_{null}), which is constructed to make the total collision frequency constant with respect to energy (ν_T).

With this, we can perform the integration in (3) analytically, without regard to the size of the time step and obtain

$$P(t) = 1 - e^{-\nu_T t}$$

so that

$$t = -\frac{\ln(1 - P(t))}{\nu_T} \tag{5}$$

For each electron we generate a uniformly distributed random variable on the interval [0,1] for the quantity $(1 - P(t))$ and use (5) to find the time when the collision will occur. We push the electrons until that time, so that we know its energy when the collision occurs. After accounting for the collision, a new collision time is calculated for the electron. The disadvantage of this method comes when we determine the type of collision that occurred; some probability exists that it will be a "null collision" in which case nothing happens. If the "null collision" probability is excessive, the efficiency of this method goes down.

Once a collision occurs, the next step is to determine the type of collision. In order to do this efficiently we generate a "stacked" table of collision frequencies as a function of energy, which is shown in Figure 2. For this example, we restrict ourselves to only three sub-process collision frequencies: the elastic $\nu_{el}(\epsilon)$, the excitational, $\nu_{ex}(\epsilon)$ and ionizing $\nu_{ion}(\epsilon)$. We stack the data by adding the data of the sub-process being plotted to all of the sub-processes plotted previously. In our example $\nu_{el}(\epsilon)$ is plotted first. The next curve is plotted by adding $\nu_{ex}(\epsilon)$ to $\nu_{el}(\epsilon)$. The next curve is plotted by adding $\nu_{ion}(\epsilon)$ to both $\nu_{ex}(\epsilon)$ and $\nu_{el}(\epsilon)$.

The dotted, vertical line in Figure 2 indicates the probability that an electron of energy ϵ_i underwent a given sub-process collision. The stacked data divides the dotted line into four segments. The fraction of the line that lies between two curves is the probability that the added process of the upper curve occurred. For example, let us generate a uniformly distributed random variable X in the interval [0,1]. If

$$\begin{aligned}
0 < X < v_{el}(\epsilon_i)/\nu_T, &\qquad \text{elastic collision} \\
v_{el}(\epsilon_i)/\nu_T < X < [v_{el}(\epsilon_i) + \nu_{ex}(\epsilon_i)]/\nu_T, &\qquad \text{excitational collision} \\
[v_{el}(\epsilon_i) + \nu_{ex}(\epsilon_i)]/\nu_T < X < [v_{el}(\epsilon_i) + \nu_{ex}(\epsilon_i) + \nu_{ion}(\epsilon_i)]/\nu_T, &\qquad \text{ionizing collision} \\
[v_{el}(\epsilon_i) + \nu_{ex}(\epsilon_i) + \nu_{ion}(\epsilon_i)]/\nu_T < X < 1, &\qquad \text{null collision}
\end{aligned}$$

If two gas species form the background neutral particles, for example nitrogen and oxygen – the main components of air, the procedure is the same as outlined above except that more bookkeeping is involved. The collision frequencies of the second gas species is stacked on top of the collision frequencies of the first gas species and the above procedure will indicate not only the sub-process, but also which gas species the electron collided with. This procedure works only because at atmospheric pressure, the various measured cross-sections are independent. At higher pressure, multiple scattering causes the measured cross sections to cross couple.

Each type of collision results in a different modification to the particle population. In an elastic collision no new particles are created. The primary electron recoils in a new

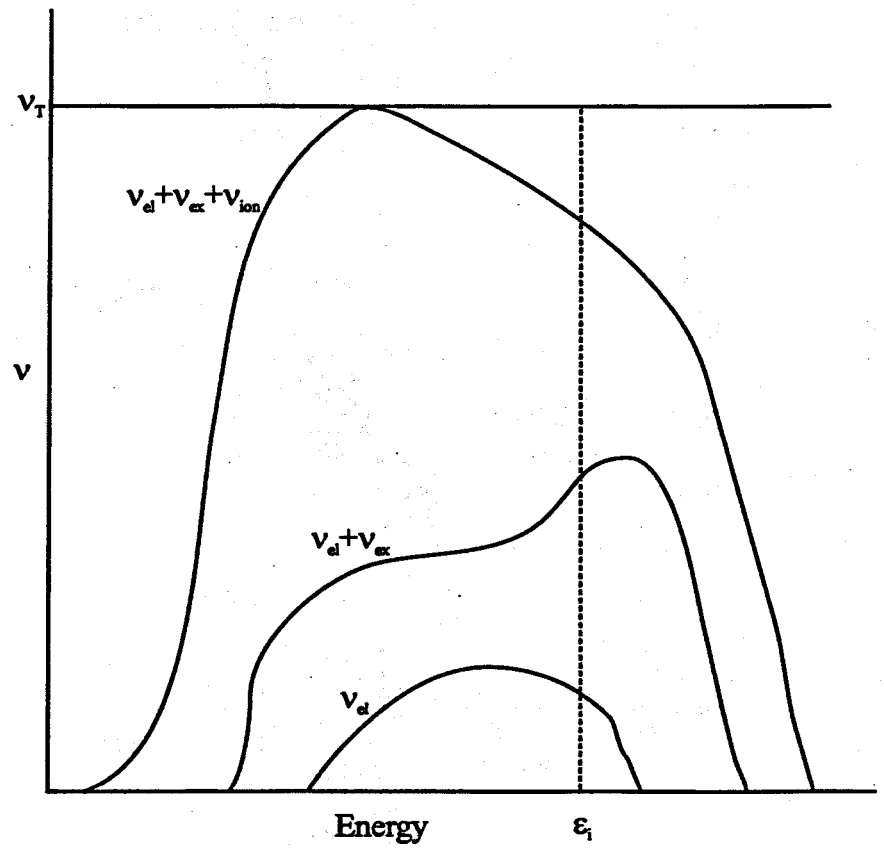

2. Stacked Collision Frequencies

random direction:

$$\theta = \cos^{-1}(1 - 2X) \tag{6}$$

and

$$\phi = 2\pi Y \tag{7}$$

where X and Y are both uniformly distributed random variables in the interval [0,1] and θ and ϕ are spherical coordinates in the center of mass coordinate system of the primary electron (x', y', z'). Figure 3 shows the center of mass coordinate system and its relationship to the laboratory coordinate system (x, y, z). In center of mass coordinates z' is along the velocity vector of the primary electron, while x' is parallel to the xy plane of the laboratory coordinates. Figure 4 shows the center of mass coordinate system looking down the z' axis in order to show ϕ more clearly. The center of mass coordinates must be transformed into laboratory coordinates using the following equations:

$$a_x = \cos\theta\cos\gamma_x - \sin\theta\cos\phi\frac{\cos\gamma_y}{\sqrt{\cos^2\gamma_x + \cos^2\gamma_y}} - \sin\theta\sin\phi\frac{\cos\gamma_z\cos\gamma_x}{\sqrt{\cos^2\gamma_x + \cos^2\gamma_y}}$$

$$a_y = \cos\theta\cos\gamma_y + \sin\theta\cos\phi\frac{\cos\gamma_x}{\sqrt{\cos^2\gamma_x + \cos^2\gamma_y}} - \sin\theta\sin\phi\frac{\cos\gamma_z\cos\gamma_y}{\sqrt{\cos^2\gamma_x + \cos^2\gamma_y}}$$

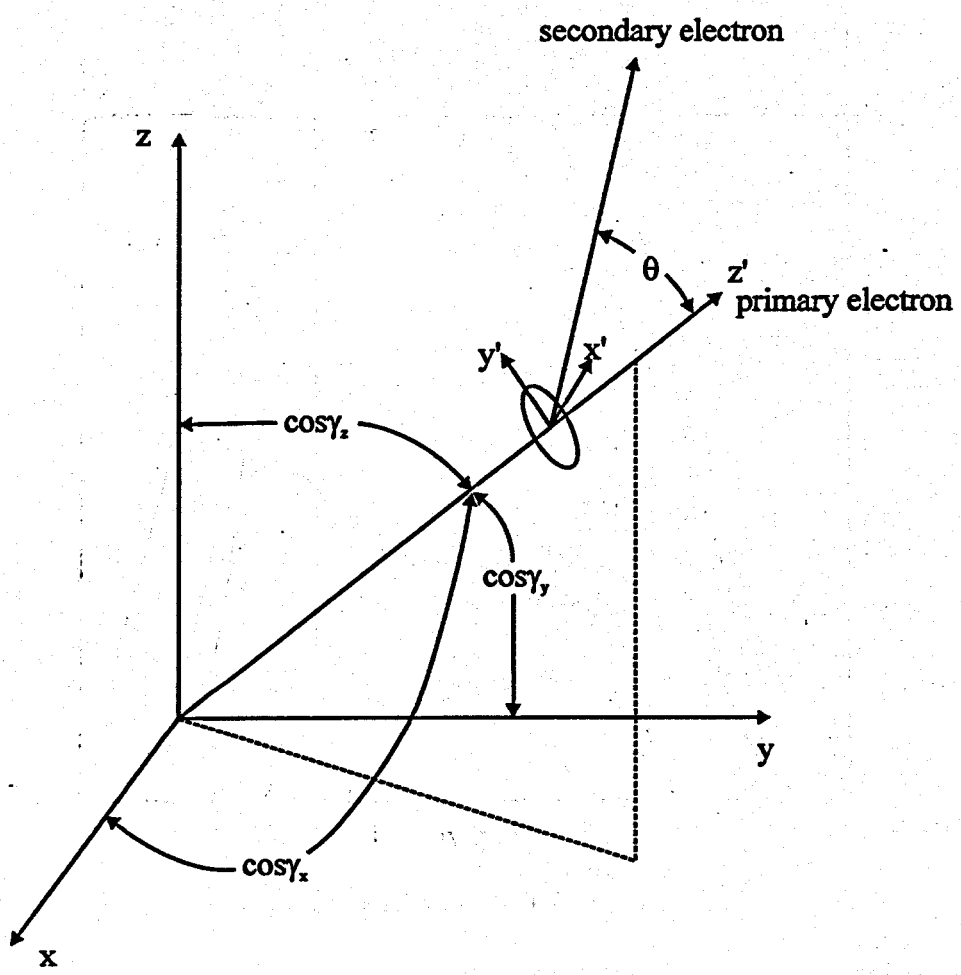

3. Center of Mass and Laboratory Coordinates

$$a_z = \cos\theta\cos\gamma_z + \sin\theta\sin\phi\sqrt{\cos^2\gamma_x + \cos^2\gamma_y}$$

where a_x, a_y, a_z is the projection of the unit vector in the center of mass coordinates on the x, y, and z coordinates of the laboratory coordinate system respectively. All other quantities are defined in Figures 3 and 4.

The energy of the primary electron is reduced after an elastic collision because a small amount of momentum is transferred to the neutral. The large differences in mass between the electron and the neutral, however, make this transfer insignificant so we choose to ignore it. An excitational collision is treated in the same manner as the elastic collision except the energy of the primary electron is reduced by the threshold energy needed to excite the neutral. This energy is obtained experimentally.

An ionizing collision results in the creation of an electron-ion pair. The energy of the primary electron is reduced by the threshold energy. The remaining energy is divided between the primary electron and the secondary electron using a uniform random variable in the interval [0,1] as the dividing fraction. For certain gases, such as nitrogen or oxygen,

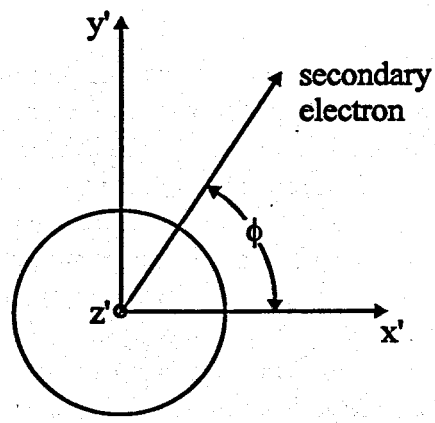

4. Center of Mass Coordinates Viewed Along Direction of Primary Electron

we have experimental data on how the energy divides [16]. The ion is given the thermal energy of the background gas. The velocity direction of the primary electron is calculated using the procedure given above for the elastic collision. The θ direction of the secondary electron is calculated using an independent choice of X in (6). The ϕ direction of the secondary electron is dependent on ϕ of the primary electron – it is offset from the primary ϕ by 180 degrees.

Both the excitational and the ionizing collision processes release photons. The photons released by excitational collisions are too low in energy to ionize any other neutrals, but they do result in visible light (in the blue region of the spectrum for the main excitational collision processes of nitrogen). The photons released by the ionizing collisions, on the other hand, have enough energy to ionize the background neutrals at various distances from the site of the collision. The tie between the ionizing collision and the photoionizing event is made experimentally by Penney and Hummert [17]. Photoionization is necessary to obtain the proper streamer velocity and to model the formation of a cathode directed streamer [4].

The procedure used to account for photoionization is now described. Using the Penney and Hummert data we can obtain the probability for creating a photo-electron anywhere in space given an ionizing collision. Therefore, after an ionizing event occurs, we generate a random number X, uniformly distributed on the interval [0,1], which we compare to the photo-electron probability (P_{pe}). If $X < P_{pe}$, an electron-ion pair due to photoionization was generated somewhere in space. If a photo-electron was generated, its distribution is uniform over 4π steradians. We use (6) and (7) to determine θ and ϕ, which in this case are already in laboratory coordinates with the origin at the collision location. The radial distance from the collision point is determined from the plot of ψ data presented in Figure 3 of [17]. The quantity ψ is the number of photo-electrons generated per (ionizing collision event - steradian cm Torr). ψ is plotted as a function of distance from the ionizing collision (R) times pressure (p) (Rp is in cm-Torr). The probability that the photo-electron is created at a distance Rp from the ionizing collision is

$$P_{pe}(Rp) = 4\pi \int_{Rp}^{\infty} \psi(r'p)\, d(r'p) \tag{8}$$

Note that P_{pe}, which we used previously, is actually $P_{pe}(0)$. Given the random number X that we generated to find if a photoionization occurred, we find the value of Rp where $P_{pe}(Rp) = X$. This represents the closest possible value of Rp where the photoionization could occur.

The photoionization event generates a second electron-ion pair in addition to the pair generated by the ionizing collision itself. The electron is given a nominal energy of 0.1 ev and a velocity direction, each component of which is uniformly distributed over the interval [-0.5,0.5] and normalized after construction. The ion, like the ion generated by the collision, is given the thermal energy of the background gas.

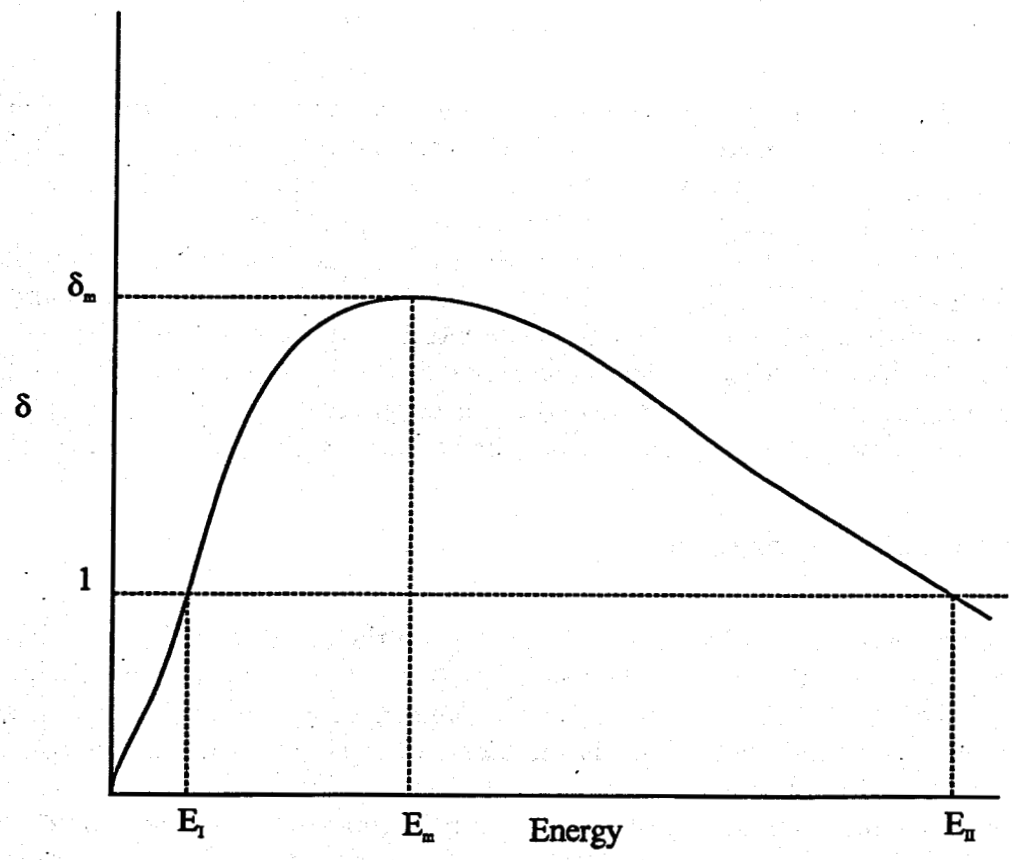

5. Secondary Electron Emission Curve

2.5 Surface Interactions

In the code, there are three ways that the electron interacts with a dielectric surface. First, the surface influences the field through an image charge, which was previously discussed. Second, the electrons are not allowed into the region occupied by the dielectric. Finally, electrons colliding with the surface either become attached to the surface or release electrons from the surface depending on the energy of the incident electron. This results in a charging of the surface, which affects the evolution of the streamer across it. This last effect, which is what we will discuss in this section, is known as secondary electron emission (SEE). The theory behind secondary electron emission of dielectrics is discussed in [18] and [19]. Figure 5 shows a typical SEE curve for a dielectric surface. The number of electrons released from the surface per incident electron (δ) is plotted as a function of the energy of the incident electron. Note that there are energies ($E < E_I$ and $E > E_{II}$) where $\delta < 1$, meaning that the incident electrons have a chance of attaching to the surface and charging it negatively. Note also that there is a maximum number of electrons released from the surface δ_m, which occurs when the incident electron has an energy of E_m. In the code we approximate the SEE curve by two straight lines. The first line passes through the points $(1, E_I)$ and (δ_m, E_m). The second line passes through the points (δ_m, E_m) and $(1, E_{II})$. In this way, we can characterize the SEE curves by four pieces of information: E_I, E_{II}, E_m

and δ_m.

If an electron hits the surface and $\delta < 1$, we generate a random variable X, uniformly distributed on the interval [0,1]. If $X < \delta$, the incident electron is moved to the surface ($x = 0$) and released back into the problem space with an energy of 0.1 ev. If $X > \delta$, the incident electron is changed to be a "wall electron", which is defined as an electron that is not allowed to move from its location on the wall. It is thus removed from the swarm, but influences the swarm through its charge. If the electron hits the surface and $\delta > 1$, we generate a number of secondaries equal to the integer part of δ. The fractional part of δ is handled like the $\delta < 1$ case. Each secondary electron is released into the problem space with an energy of 0.1 ev. For each secondary electron created, a corresponding "wall ion" is created that is not allowed to move from the wall, but influences the swarm through its charge.

2.6 Particle Renormalization

The breakdown process involves electron densities on the order of $10^{14} - 10^{15}$ electrons/cm^3. On the computers available to us, our simulation size is limited to approximately 10^4 particles. Therefore, each particle represents some number of electrons or ions depending on the stage of the simulation. This is similar to what is done when simulating a collision between two galaxies [12] except that in our case the number of particles grows exponentially throughout the simulation and must be renormalized repeatedly as time progresses [14]. For example, in the first results presented below, at 11 ns there are 10^9 electrons in the problem space; each particle represents an average of 10^5 electrons if we are using 10^4 particles to simulate the electrons.

Electrons and ions are renormalized separately and the renormalization is accomplished using energy as a discriminator. In this code, prior to running the problem, the user defines three energy bins: low energy, medium energy and high energy by defining the upper and lower limits of the medium energy bin and by defining the number of particles that will remain in each of the energy bins once the renormalization has taken place. When the number of electrons reaches a given, user-defined limit, the particles representing the electrons are listed in energy order from the electrons having the lowest energy to the electrons having the highest energy. This allows us to calculate how many electron particles are in each energy bin. The number of electron particles in each energy bin is then reduced to the bin limit by eliminating electrons uniformly over the bin's energy range. This culling of the particles is done without regard to spatial distribution of the particles. The charge of each of the particles that are left in the energy bin is multiplied by the reciprocal of the reduction factor so that the total number of electrons represented remains the same. For example, if the low energy bin contains 1000 particles and we want to renormalize to 750 particles, we eliminate every fourth particle in the energy-ordered list over this energy range. We then multiply the charge in the remaining particles by 4/3 so that the remaining 750 particles still represent the original 1000 particles. The thought behind this renormalization scheme is that the energy bins are defined so that over the course of the simulation more particles are dedicated to modeling the higher energy

electrons and less to modeling the lower energy electrons. The high energy electrons reside in the head of the streamer making them more important to the physics of breakdown than the low energy electrons, which reside in the streamer's tail.

The ions are created at thermal background energy and not allowed to move throughout the simulation. Therefore, all of the ions will reside in the low energy bin and be renormalized in accordance with its parameters.

3 Results

The results show the evolution of a cluster of ten electrons initially confined to a sphere 1 μm in radius. At $t = 0$, the electrons are released and are subsequently pushed by the field, collide and avalanche. The number of electrons or ions that triggers renormalization was set to 14,000, so we could have up to 28,000 particles existing simultaneously in the problem space. The low energy bin ranged from 0 to 15 ev and contained 5000 particles after renormalization. The medium energy bin ranged from 15 ev to 250 ev and contained 2000 particles after renormalization. Finally, the high energy bin ranged from 250 ev to infinity and contained 1000 particles after renormalization. The background gas was pure nitrogen having a temperature of 0.01 ev.

3.1 Breakdown Through a Volume, Photoionization Off

The first set of results (Figures 6-10) have the photoionization effect turned off. The incident field was set to be -3 MV/m and the density of the nitrogen was set to be $1.0 \times 10^{25}\text{m}^{-3}$ – about one third of an atmosphere. The solid curve in Figure 6 shows the number of electrons as a function of time. The dashed curve is a straight line, which is a plot of the function $n = 10 \cdot e^{2.035t}$, where t is in nanoseconds. In the region between 0 and 7 ns, the exponential growth in the number of electrons indicates that the electrons are avalanching. At approximately 7 ns the growth in the number electrons begins to slow down from strict exponential behavior, which indicates the onset of streamering [3]. Figure 7 shows the E_z field at each electron in the swarm as a function of the z location of each electron at $t = 9.911$ ns (after the streamer is formed). The head of the streamer is between 2900 μm and 3100 μm, while the body of the streamer is between 2200 μm and 2800 μm. As expected, the field in the streamer head is enhanced over the applied field by a factor of 1.5 to 2 and the field in the streamer body is reduced by a factor of approximately 0.5 from the applied field [3]. Since photoionization is turned off, the streamer propagates only in the anode direction. Figures 8, 9 and 10 show three orthogonal views of the electrons at $t = 9.911$ ns to give an idea of the swarm appearance.

3.2 Breakdown Through a Volume, Photoionization On

The next set of results has the photoionization effect turned on. The incident field was set to be -8.06 MV/m and the density of the nitrogen was set to be 2.686×10^{25} m^{-3}– one

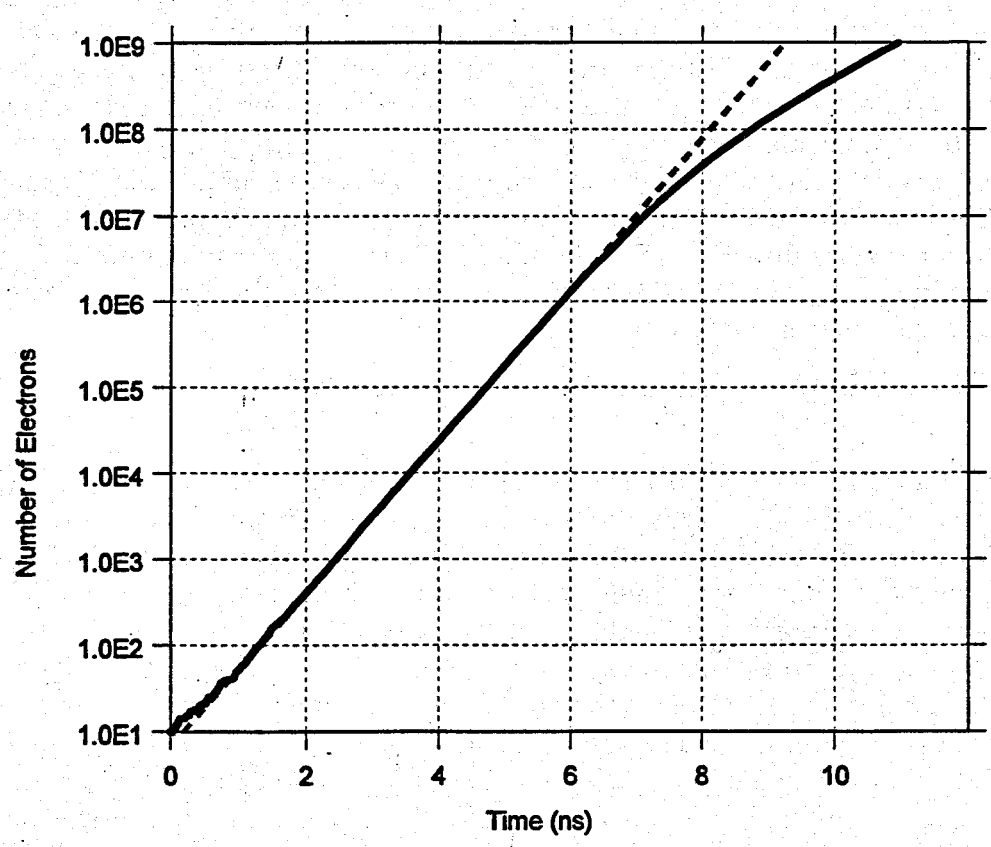

6. Number of Electrons vs. Time

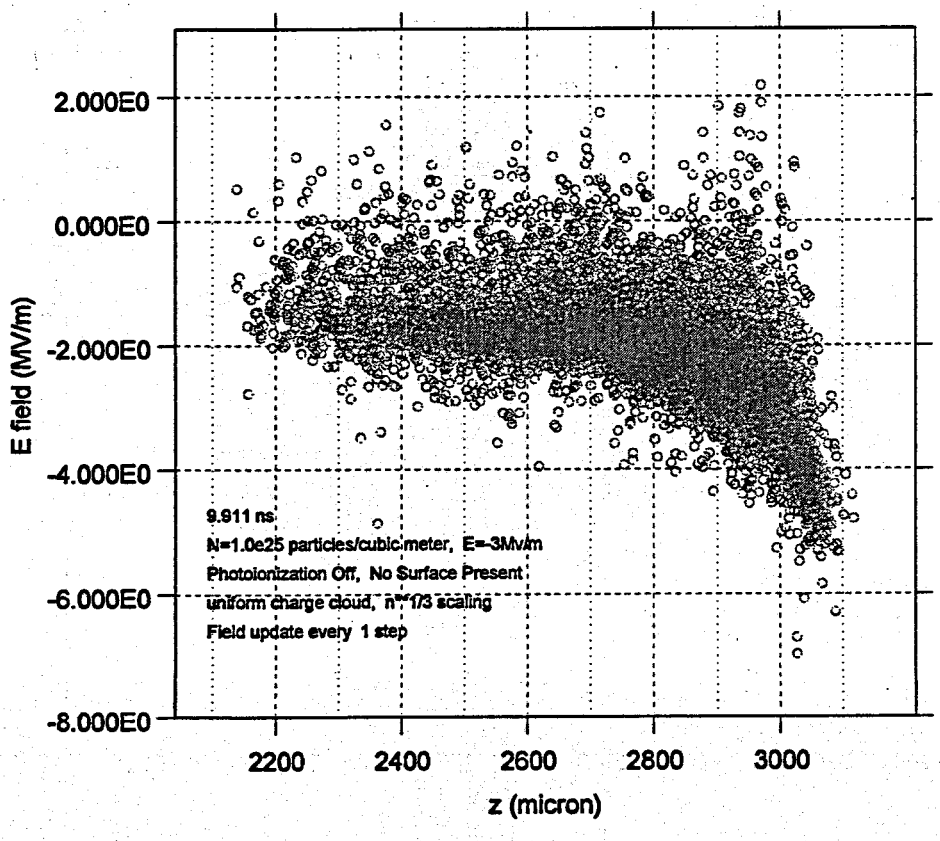

7. E_z at Each Electron vs. z

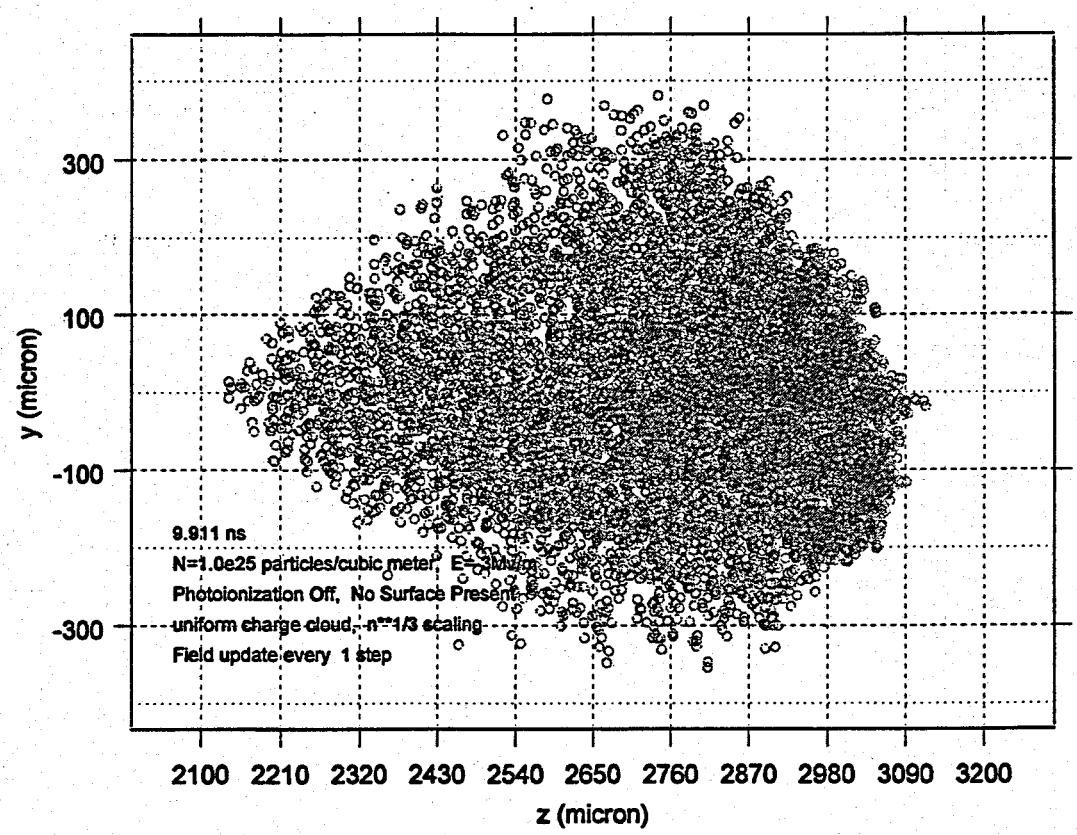

8. Electron Cloud as Viewed Along $\hat{x}$

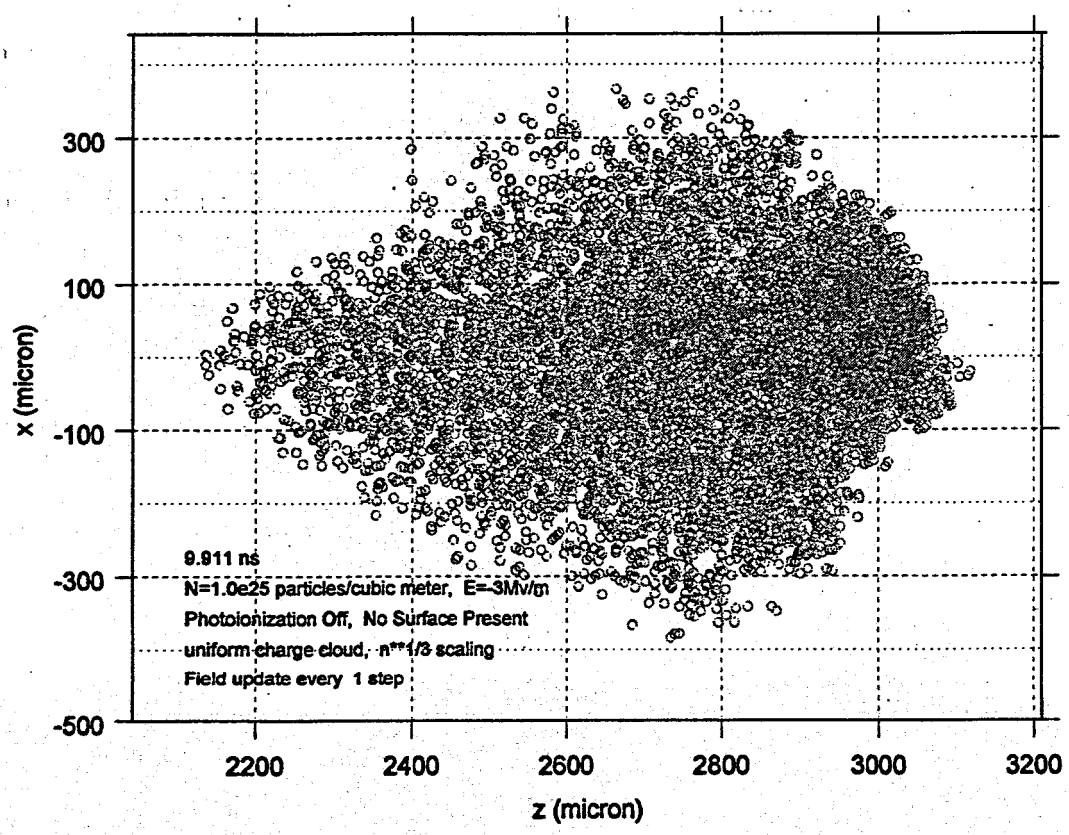

9. Electron Cloud as Viewed Along $\hat{y}$

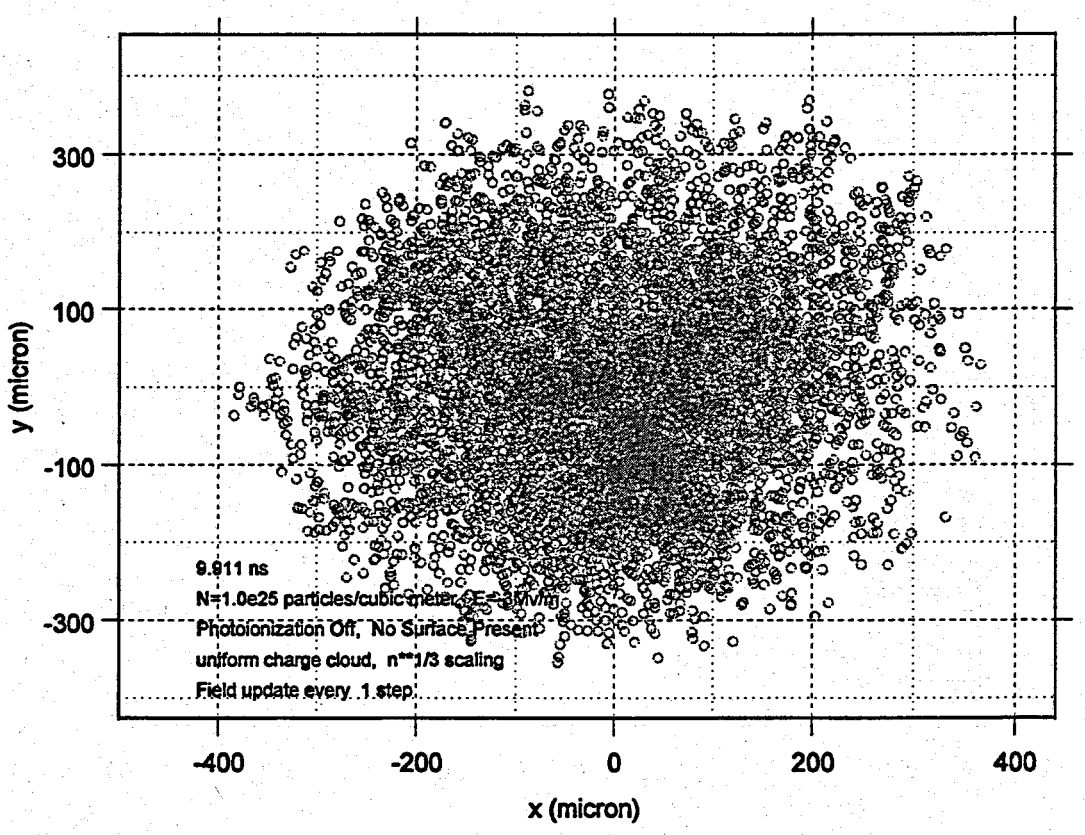

10. Electron Cloud as Viewed Along $\hat{z}$

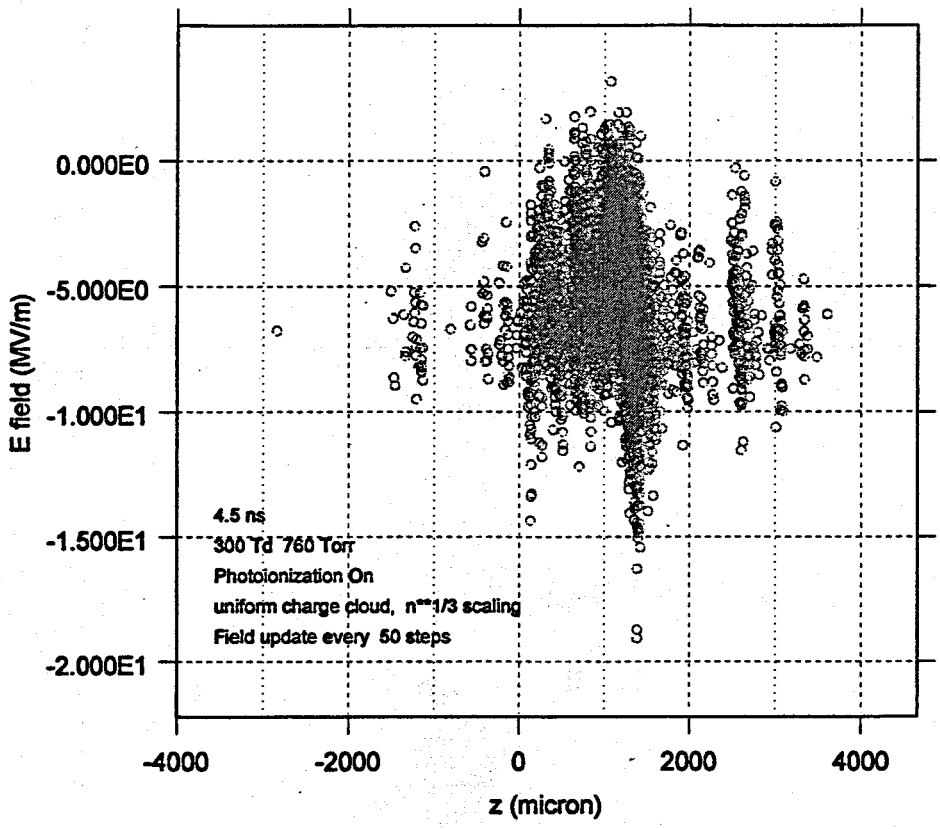

11. E_z at Each Electron vs. z with Photoionization On

atmosphere. Figure 11 shows E_z field at each electron in the swarm as a function of the z location of each electron at $t = 4.5$ ns. Several avalanches have formed and transitioned to streamers.

Figure 12 shows how the streamers are developing spatially. Instead of a single plume of electrons as was the case when the photoionization was turned off, electrons are avalanching and forming streamers throughout the space. Although each individual electron is moving toward the anode, the formation of new avalanching electrons displaced from the original avalanche in the direction of the cathode ($-z$) makes it appear as the streamers coalesce that the streamer is cathode directed as well as being anode directed.

4 Experiments

This project was planned to run for two years. Validation experiments were to be performed at Stevens Institute of Technology in the second year. The experiments were to

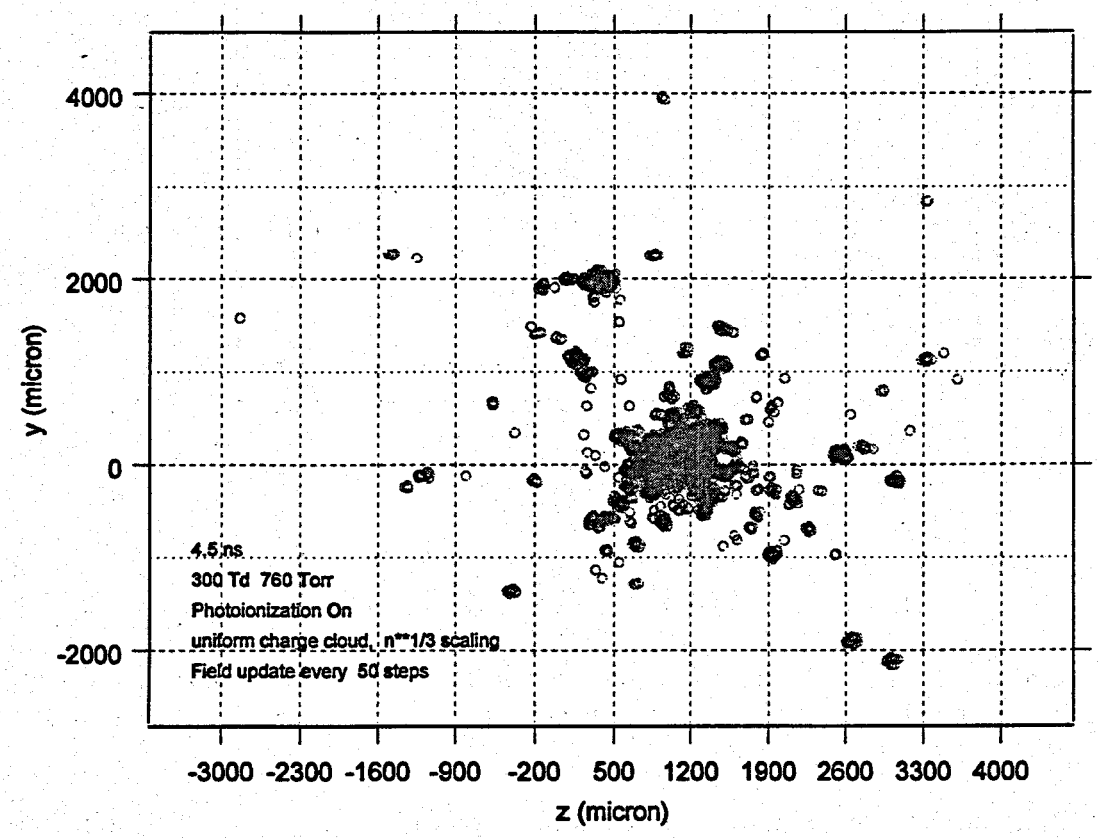

12. Electron Cloud as Viewed Along $\hat{x}$ with Photoionization On

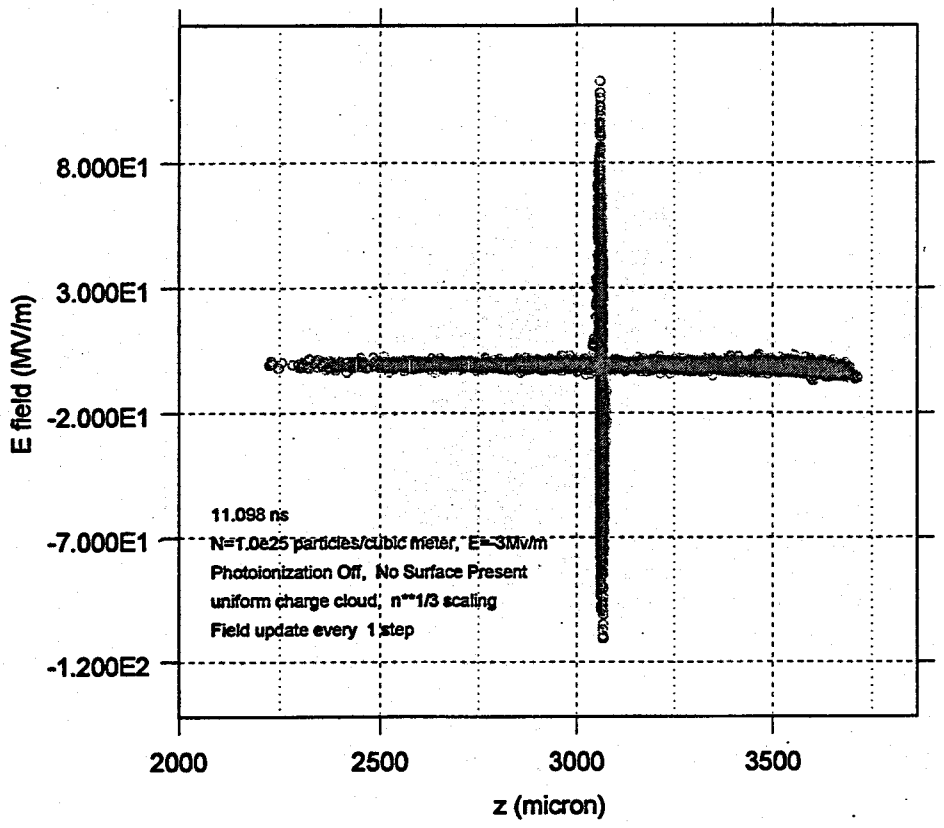

13. E_z at Each Electron vs. z Showing Onset of Instability

measure the velocity of the streamer as it traveled across a dielectric surface as a function of gap distance and gas pressure and compare these to the code run. As a result of budget cuts in the overall LDRD program, this project was terminated at the beginning of the second year and the experiments were subsequently cancelled.

5 Problem Areas

A major problem, that we hadn't found the solution to when the project was terminated is shown in Figure 13, which is the same streamer as the one in Figure 7, but at a later time ($t = 11.08$ ns). In a region in the body of the streamer, we observe a high, non-physical electric field at a few of the electrons. These electrons avalanche and create more electrons in the same region, which also are subject to the high electric field. In a very short time after the onset of the instability, the slope of Figure 6 ceases to decrease and actually exhibits super exponential growth.

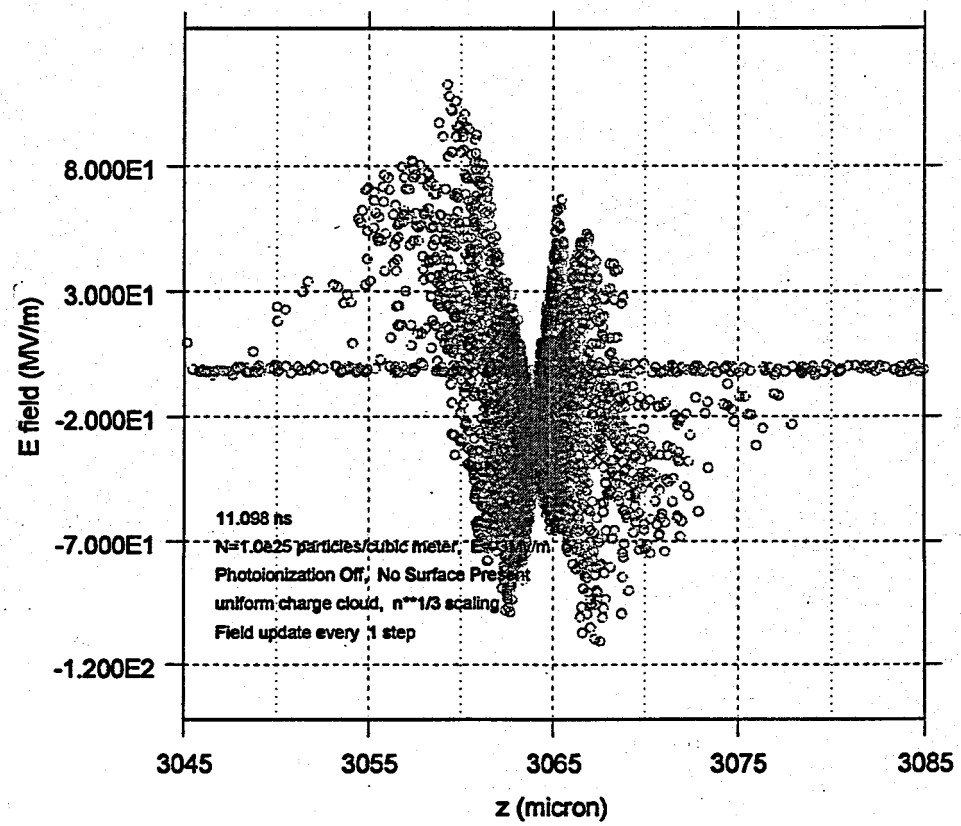

14. Detail of Instability Region

A detailed view of the region around the instability is shown in Figure 14. We did not discover the cause of this instability, but just prior to its onset, the electrons form a dense cluster at the location where the instability eventually occurs.

We attempted to suppress the instability by smoothing the electric field in the body region of the streamer. Our conjecture was that repeated renormalization of the electrons in the body region caused the neutral plasma behind the streamer head to become artificially inhomogeneous. Our most successful attempt at smoothing was realized by replacing the point charges in the $\overline{E}$ field calculation with uniform charge clouds whose radii are allowed to vary such that the density of charge inside the cloud remained constant at a user-defined value. In other words, the charge associated with a source twig in the tree is no longer concentrated at the center of charge location, but is uniformly distributed over the volume of a sphere. Similarly, the charge associated with the observation electron is also uniformly distributed over the volume of a sphere.

The expression for the mean $\overline{E}$ field due to charge cloud interaction is more complicated

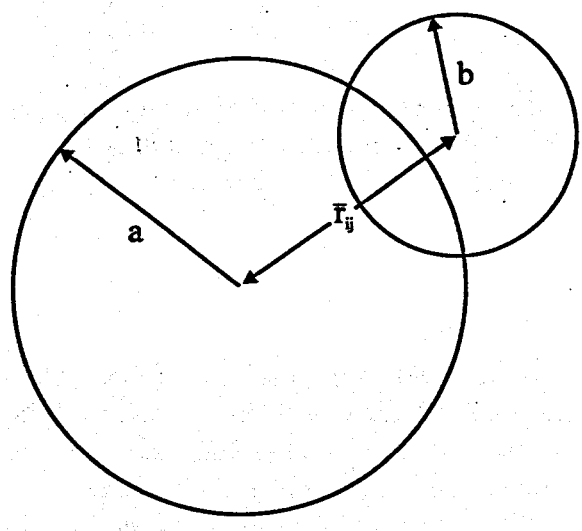

15. Source and Observation Clouds

than (2). Assuming that the two charge clouds in question have a radius of a and b respectively and that they are separated by a distance $|\overline{r_{ij}}|$ as shown in Figure 15,if there is partial overlap between the two charge clouds (the situation actually shown in Figure 15), (2) becomes

$$\overline{E_j}(i) = \frac{q_j}{4\pi\varepsilon_0}\frac{\overline{r_{ij}}}{32|\overline{r_{ij}}|^3 b^3 a^3}\left[|\overline{r_{ij}}|^6 - 9\left(b^2+a^2\right)|\overline{r_{ij}}|^4 + 16\left(b^3+a^3\right)|\overline{r_{ij}}|^3\right. \tag{9}$$

$$\left. -9\left(a^2-b^2\right)^2|\overline{r_{ij}}|^2 + \left(a^2+4ab+b^2\right)(a-b)^4\right], \; |b-a| < |\overline{r_{ij}}| < b+a$$

If one charge cloud is completely contained within the other, (2) becomes

$$\overline{E_j}(i) = \frac{q_j}{4\pi\varepsilon_0}\frac{\overline{r_{ij}}}{\max(a,b)^3}, \; 0 < |\overline{r_{ij}}| < |b-a|$$

Finally, if the charge clouds do not intersect each other, (2) does not change, i.e.,

$$\overline{E_j}(i) = \frac{q_j}{4\pi\varepsilon_0}\frac{\overline{r_{ij}}}{|\overline{r_{ij}}|^3}, \; |\overline{r_{ij}}| > b+a$$

If the radii of the two charge clouds are the same ($b = a$), Equation (9) simplifies to

$$\overline{E_j}(i) = \frac{q_j}{4\pi\varepsilon_0}\frac{\overline{r_{ij}}}{32a^6}\left[32a^3 - 18a^2|\overline{r_{ij}}| + |\overline{r_{ij}}|^3\right], \; 0 < |\overline{r_{ij}}| < 2a$$

The expression for radius a is

$$a = \sqrt[3]{\frac{3n_a}{4\pi n_e}}$$

where n_a is the number of charged particles represented by the charge cloud and n_e is the chosen charge density. For all of our results we used $n_e = 10^{14}$ cm^{-3} because this is the charge particle density we expect inside the head of a streamer. Radius b is calculated

similarly.

Prior to use of the charge clouds, the simulation was going unstable 1 or 2 ns after the onset of streamering. With the use of the charge clouds the instability was delayed to occur at 4 to 5 seconds after the onset of streamering.

6 Future Work

If this work were to be continued sometime in the future, the most important unresolved issue is to study and solve the instability problem. Unless the instability problem is solved, we will be unable to progress to simulate branching of the streamer or progress toward simulating the formation of an arc. Also, when photoionization is turned on, the instability occurs before the various streamers in the problem space have had a chance to coalesce and form definite cathode and anode directed streamer fronts. Without this information we can't compare simulations results to the velocity measured in a validation experiment. Once the instability is cured, the second most important issue is to perform the planned validation experiments to give us some confidence in the code.

The third issue is to perform a series of experiments to determine if a dielectric photoelectric effect exists and if it is important in the breakdown process. Recall that although excitational collisions emitted visible light and nonionizing ultraviolet light, only the ionizing collisions emitted photons with enough energy to photoionize additional neutrals. If a dielectric surface is present, however, lower energy photons could cause the surface to emit electrons due to a photoelectric effect. This could be a major contributor in the surface breakdown process.

The fourth issue is to correct our cross section data for oxygen and run some validation tests in oxygen. Unlike nitrogen, oxygen has an attachment mechanism – electrons attach to oxygen neutrals – which suppresses the growth of the number of electrons. Finally, we need to simulate breakdown in a nitrogen-oxygen mix (simulating air) and run some validation tests in the mixture.

7 Conclusion

In this project we used a computer code to successfully simulate the transition from avalanche to streamer in three dimensions. It is our belief that this is the first time this has been done. We were unable to simulate the formation of branching because of an instability that occurred after the streamer was formed. Further work on the instability, as well as the planned validation experiments, were stopped as a result of the premature termination of this project..

References

[1] Bazelyan, E. M. and Raizer, Yu. P., *Spark Discharge*, CRC Press, Boca Raton, 1997, p. 11.

[2] Nasser, E., *Fundamentals of Gaseous Ionization and Plasma Electronics*, Wiley, New York, 1971, pp. 68-69, 264-268.

[3] Lagarkov, A. N. and Rutkevich, I. M., *Ionization Waves in Electrical Breakdown of Gases*, Springer-Verlag, New York, 1993, pp. 3-11.

[4] Kunhardt, E. E.,, Tzeng, Y. "Development of an electron avalanche and its transition into streamers", *Phy. Rev. A*, v. 38, no. 3, Aug. 1988, pp. 1410-1421.

[5] Maxtadt, F. W., "Insulator arcover in air", *Trans. A.I.E.E.* July 1934, pp.1062-1068.

[6] Miller, H. C., "Surface flashover of insulators", *IEEE Trans. on Electrical Insulation*, v. 24, no. 6, Oct. 1989, pp. 765-786.

[7] Latham, R.(ed.), *High Voltage Vacuum Insulation*, Academic Press, 1995, pp. 166-183.

[8] Anderson, R. A., Brainard, J. P., "Mechanism of pulsed surface flashover involving electron-stimulated desorption", *J. Appl. Phys*, 51 (3), March 1980, pp. 1414-1421.

[9] Neuber, A., Butcher, M., Krompholz, H., Hatfield, L. L., Kristiansen, M., "The role of outgassing in surface flashover under vacuum", *12th Int. Pulsed Power Conf., Monterey, CA*, 1999, pp. 1-5.

[10] Birdsall, C. K. and Langdon, A. B., *Plasma Physics via Computer Simulation*, Institute of Physics Publishing, Bristol, 1998, pp.7-27.

[11] Hockney, R. W. and Eastwood, J. W., *Computer Simulation Using Particles*, Institute of Physics Publishing, Bristol, 1994, pp.24-43.

[12] Pfalzner, S. and Gibbon, P., *Many-Body Tree Methods in Physics*, Cambridge University Press, 1996, pp. 9-26, 37-46.

[13] Vahedi, V. and Surendra, M., "A monte-carlo collision model for the particle-in-cell method: applications to argon and oxygen discharges", *Computer Physics Communications*, 84 (1995), pp. 179-198.

[14] Kunhardt, E. E. and Tzeng, Y., "Monte carlo technique for simulating the evolution of an assembly of particles increasing in number", J. Comp. Phys., 67, 1986, pp. 279-289.

[15] Lin, S. L., and Bardsley, J. N., "The null-event method in computer simulation", *Computer Physics Communications*, 15 (1978) pp. 161-163.

[16] Opal, C. B., Peterson, W. K. and Beaty, E. C., "Measurements of secondary-electron spectra produced by electron impact ionization of a number of simple gases", *Jour. Chem. Phys.*, v. 55, no. 8, 1971, pp. 4100-4106.

[17] Penney, G. W. and Hummert, G. T., "Photoionization measurements in air, oxygen and nitrogen", *Jour. App. Phys.*, v. 41, no. 2, 1970, pp. 572-577.

[18] Scholtz, J. J., Kijkkamp, D. and Schmitz, R. W. A., "Secondary electron emission properties", *Philips J. Res.*, 50 (1996), pp. 375-389.

[19] Deswart, S. T., Van Gorkom, G. G. P., Hendriks, B. H. W., Lambert, N. and Trompenaars, P. H. F., "Basics of electron transport over insulators", *Philips J. Res.*, 50 (1996), pp. 307-345.

Distribution:

1 Prof. Erich E. Kunhardt
807 Castle Terrace
Hoboken, NJ 07030

1 ITT Industries/AES
ATTN: K.S.H. Lee
1033 Gayley Ave.
Suite 215
Los Angeles, CA 90024

1	MS0188	LDRD Office, 01030
9	MS1152	R. E. Jorgenson, 01642
5	MS1152	L. K. Warne, 01642
1	MS1152	M. L. Kiefer, 01642
1	MS1152	K. O. Merewether, 01642
1	MS1152	D. B. Seidel, 01642
1	MS1152	M. A. Dinallo, 01643
1	MS1194	T. D. Pointon, 01644
1	MS1111	H. P. Hjalmarson, 09235
1	MS0888	R. A. Anderson, 01846
1	MS9018	Central Technical files, 8945-1
2	MS0899	Technical Library, 09616
1	MS0612	Review & Approval Desk, 09612 For DOE/OSTI